

Light absorption coefficients of ionic liquids under electric field

Ji Zhou(周吉), Shi-Kui Dong(董士奎), Zhi-Hong He(贺志宏), Ju-Lius Caesar Puoza, Yan-Hu Zhang(张彦虎)

Citation: Chin. Phys. B . 2019, 28(1): 017801. **doi:** 10.1088/1674-1056/28/1/017801
Journal homepage: http://cpb.iphy.ac.cn; http://iopscience.iop.org/cpb

What follows is a list of articles you may be interested in

Particle swarm optimization and its application to the design of a compact tunable guided-mode resonant filter

Dan-Yan Wang(王丹燕), Qing-Kang Wang(王庆康)
Chin. Phys. B . 2018, 27(3): 037801. **doi:** 10.1088/1674-1056/27/3/037801

Effect of size and indium-composition on linear and nonlinear optical absorption of InGaN/GaN lens-shaped quantum dot

Ahmed S Jbara, Zulkafli Othaman, M A Saeed
Chin. Phys. B . 2016, 25(5): 057801. **doi:** 10.1088/1674-1056/25/5/057801

Design of broad angular phase retarders for the complete polarization analysis of extreme ultraviolet radiation

Lin Cheng-You, Chen Shu-Jing, Chen Zhao-Yang, Ding Ying-Chun
Chin. Phys. B . 2015, 24(11): 117802. **doi:** 10.1088/1674-1056/24/11/117802

Nonlinear optical characterization of phosphate glasses based on ZnO using the Z-scan technique

Masoumeh Shokati Mojdehi, Wan Mahmood Mat Yunus, Khor Shing Fhan, Zainal Abidin Talib, N. Tamchek
Chin. Phys. B . 2013, 22(11): 117802. **doi:** 10.1088/1674-1056/22/11/117802

The effect of an optical pump on the absorption coefficient of magnesium-doped near-stoichiometric lithium niobate in terahertz range

Zuo Zhi-Gao, Ling Fu-Ri, Ma De-Cai, Wu Liang, Liu Jin-Song, Yao Jian-Quan
Chin. Phys. B . 2013, 22(10): 107802. **doi:** 10.1088/1674-1056/22/10/107802

Light absorption coefficients of ionic liquids under electric field*

Ji Zhou(周吉)[1], Shi-Kui Dong(董士奎)[2], Zhi-Hong He(贺志宏)[2], Ju-Lius Caesar Puoza[3], and Yan-Hu Zhang(张彦虎)[4,†]

[1] *Beijing Institute of Space Mechanics & Electricity, Beijing* 100094, *China*
[2] *School of Energy Science and Engineering, Harbin Institute of Technology, Harbin* 150001, *China*
[3] *Department of Mechanical Engineering, Sunyani Technical University, P. O. Box* 206, *Sunyani, Ghana*
[4] *Advancd Manufacturing & Equipment Institute, Jiangsu University, Zhenjiang* 212013, *China*

(Received 29 June 2018; revised manuscript received 10 November 2018; published online 25 December 2018)

Ionic liquids have attracted a lot of research attention for their applications in novel optoelectronic structures and devices as an optical means of regulating electricity. Although the electro-optic effect of ionic liquids is mentioned in some literature, quantitative testing and analysis are hardly found in light absorption coefficients of ionic liquids under an electric field. In the present study, an experimental apparatus is designed to measure the absorption coefficients of ionic liquids under different electric fields. Five groups of imidazole ionic liquids are experimentally investigated and an inversion is performed to determine the spectral absorption coefficients of the imidazole ionic liquids under the electric fields. Different intensities with multiple interface refractions and reflections are also considered, and the various measurement errors are analyzed through uncertainties propagation analysis. Spectral absorptions of ionic liquids from 300 nm to 2500 nm are obtained and the absorption coefficients are retrieved. It is found that the absorption behavior of ionic liquids changes in some frequency bands under an applied electric field. The experimental results show that the absorption coefficient of the ionic liquid increases with the voltage increasing at 1520 nm and 1920 nm. The change rate is affected by the types of anions and cations in the ionic liquid and the diffusion rate of the ions therein. This study provides illustrations for the ionic liquid-based electro-optical regulation in terms of physical property parameters and the testing technique.

Keywords: ionic liquid, absorption coefficient, electro-optical property, uncertainty propagation analysis

PACS: 78.40.–q, 78.20.Ci, 33.57.+c, 78.20.Jq **DOI:** 10.1088/1674-1056/28/1/017801

1. Introduction

Ionic liquid, called room temperature molten salt, is a new kind of electro-optical material which differs from dielectrics and semiconductors. It has excellent electric, magnetic, acoustic, thermal, and optical properties. Ionic liquid can be mixed or combined with some hard materials to form various novel superconducting materials with unique electro-optical, magneto-optical, and/or thermo-optical properties. Ionic liquid has been designated as a promising functional material in the 21st century. Relevant studies[1,2] showed that an ionic liquid enables wide-spectrum electro-optical regulation by optical means. The optical transmission behavior of the ionic liquid in an applied field is of great significance for promoting the application in the electro-optical regulation field.

Room-temperature imidazole ionic liquid has received considerable attention in recent years because it can be substituted for volatile organic compounds and is widely used in synthesis, catalysis, electrochemistry, and optical physics.[3–6] The optical absorption properties have been studied extensively. For instance, Du *et al.*[7] explored the explicit correlation between the structural and optical properties of an imidazolium amino acid-based ionic liquid. Their results showed that the absorption behaviors of imidazolium-based ionic liquids are sensitive to the local heterogeneous environments. Song *et al.*[8] measured the UV spectrum of 1-methyl-3-butyl imidazole tetrafluoroborate in water in a spectral range of 200–400 nm and found that the maximum light absorption wavelength is 221 nm. Yang[9] and Yu *et al.*[10] also explored the UV-spectrum absorption behavior of 1-methyl-3-butyl imidazole nitrate in ethanol and water. Paul *et al.*[11–13] presented the light absorption and fluorescence behaviors of a series of imidazole ionic liquids within ultraviolet and visible spectra. Their findings indicated that the light absorption of PF6/BF4-based imidazole ionic liquids is indeed not negligible, differing from the conventional transparent medium. Furthermore, the maximum fluorescence values depend heavily on the wavelength of the excitement wave. Jo *et al.*[14] studied the emissivity differences of ionic liquids of pyridine (quaternary ammonium) salts with different radicals at position 2 at different wavelengths. Zhang *et al.*[15] experimentally examined the radiation properties of [Hmim][Tf2N] ionic liquid and its nanofluid. Their findings demonstrated that [Hmim][Tf2N] is nearly transparent in the visible spectrum, and its light absorption property is dramatically improved due to some nanoparticles scattered within. Ansari *et al.*[16] explored the light absorption and emission properties of binary lanthanide/nitrate

*Project supported by the National Natural Science Foundation of China (Grant Nos. 51576054 and 51705210).
†Corresponding author. E-mail: zhyh@ujs.edu.cn
© 2019 Chinese Physical Society and IOP Publishing Ltd

complex and ternary lanthanide/nitrate/chloride complex in a water-bearing ionic liquid.

Interestingly, Hu *et al.*[17] developed a composite material with unique electro-optical properties. Under an electric field, the material can provide a chiral radical density gradient distribution, resulting in broadband reflection and three states of transition which are of transparency, diffuse reflection, and mirror reflection. This technology has a potential application in smart glass and electronic paper. Besides, Wang *et al.*[2] revealed that ultra-high-density electron holes and their electro-optical regulation within the far infrared and visible spectra, which provides an approach to developing the large-area electrochromic smart window used in energy-saving buildings and vehicles. Nakano *et al.*[18] invented a VO_2-based infrared-sensitive field-effect device, which can serve as an electric switch for light transmittance and conventional current for the voltage regulation and thermal cutting filter. Reddy *et al.*[19] developed a novel electrochromic device that is synthesized in a hydrophobic ionic liquid and each cathode and anode consisted of a thermally stable plasma substrate. He *et al.*[20] studied the electro-optic effect of the imidazole ionic liquid in the optofluidic waveguide. The results showed that the absorption behavior is attributed to the imidazole part and relevant structures. In addition, both the regulation range and response speed increase with the increasing of the voltage and the electrical conductivity of the ionic liquid.

From the above-mentioned research, very little is known about the accuracy and error of absorption coefficient measurements in the scope of light absorption behavior of ionic liquids. Specifically, there is no report on the analysis of propagated uncertainties in measurement results affected by multiple measurement factors. Moreover, the knowledge of the electro-optic property changes of ionic liquids under an applied electric field is limited. For the optical parameters in an electrical field, it is currently impossible to quantitatively identify the influence of the types of cations and anions and carbon chain length on the optical properties of ionic liquids, i.e., their absorption coefficients. This hinders the further development and application of ionic liquids.

In this study, an inversion is performed on the spectral transmittance measurements to identify the absorption coefficient versus external voltage relation, with multiple interface refractions and reflections considered. Additionally, the analysis of propagated uncertainties is carried out to identify the effects of different errors on the light absorption coefficient inversion results. Finally, an experimental measurement program based on the transmission method is designed for C_3MImI (methyl propyl imidazole iodide) and its four derivatives including C_5MImI (methyl pentyl imidazole iodide), C_4MImI (methyl butyl imidazole iodide), C_3MImBr (methyl propyl imidazole bromide), and C_3MImBF_4 (methyl propyl imidazole tetrafluoroborate). This study is of great significance for accurately measuring the ionic liquids' absorption coefficients and promoting their application in the electro-optic regulation field.

2. Theoretical analysis

2.1. Ionic liquid's absorption coefficient inversion

In the experiment of spectral transmittance, an inversion model is necessary to determine the absorption coefficient. In the process, the influences of the sample tank and interface refractions need to be considered. The light transmission process of the empty glass tank and that of the liquid-containing glass tank are illustrated by a single-layer model and a double-layer model, respectively, as shown in Fig. 1. In Fig. 1, α_1 is the absorption ratio of glass when there is no liquid in the tank, α_2 is the absorption ratio of glass when there is liquid in the tank, α_3 is the absorption ratio of liquid when there is liquid in the tank, τ_1 and τ_2 are the transmittances of the lower surface and upper surface of the glass tank, respectively, τ_3 and τ_4 are the transmittances of the lower surface and upper surface of the liquid-containing glass tank, respectively, τ_5 is the transmittance of the upper surface of the liquid-containing glass tank, R_1 is the reflectance between glass and air when light enters from air into glass, R_2 is the reflectance between air and glass when light enters from glass into air, R_3 is the reflectance between glass and liquid, and R_4 is the reflectance between air and liquid.

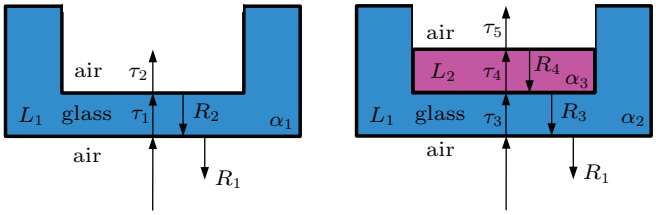


Fig. 1. Illustration of physical models for transmittance: (a) single-layer model and (b) double-layer model.

Light always strikes perpendicularly on the interfaces in the entire measurement process. Then, the reflectance of light into the glass from the air is equal to that of light into the air from the glass. For the double-layer model, the reflectance can be expressed as

$$\begin{cases} R_1 = R_2 = \left[\left(n_{\text{glass}} - n_{\text{air}}\right)/\left(n_{\text{glass}} + n_{\text{air}}\right)\right]^2, \\ R_3 = \left[\left(n_{\text{glass}} - n_{\text{liquid}}\right)/\left(n_{\text{glass}} + n_{\text{liquid}}\right)\right]^2, \\ R_4 = \left[\left(n_{\text{liquid}} - n_{\text{air}}\right)/\left(n_{\text{liquid}} + n_{\text{air}}\right)\right]^2, \end{cases} \tag{1}$$

where n_{liquid} is the refractive index of the measured liquid, n_{glass} is the refractive index of the sample tank, and n_{air} is the refractive index of the air and assumed to be 1 in this research. In the absorption coefficient inversion process, multiple reflections and refractions in the media are considered.

The transmittance of the empty glass tank (without liquid) is calculated from[21]

$$\tau_2=(1-\alpha_1)(1-R_1)(1-R_2)/\left[1-R_1R_2(1-\alpha_1)^2\right]. \quad (2)$$

When the glass tank contains liquid, multiple interfaces are involved and the physical model is shown in Fig. 2. The model consists of two layers (b, $b+1$), and the following expressions can be determined and obtained through derivation operation:

$$\begin{cases} F_{A_b}^{B_b} = \dfrac{\exp(-k_bL_b)}{[1-R_BR_A\exp(-2k_bL_b)]}, \\ F_{B_b}^{B_b} = R_A\dfrac{\exp(-2k_bL_b)}{[1-R_BR_A\exp(-2k_bL_b)]}, \\ F_{B_{b+1}}^{B_{b+1}} = R_C\dfrac{\exp(-2k_{b+1}L_{b+1})}{[1-R_BR_C\exp(-2k_{b+1}L_{b+1})]}, \\ F_{B_{b+1}}^{C_{b+1}} = \dfrac{\exp(-k_{b+1}L_{b+1})}{[1-R_BR_C\exp(-2k_{b+1}L_{b+1})]}, \end{cases} \quad (3)$$

where $F_{A_b}^{B_b}$ indicates the proportion of energy that passes through interface A and arrives at the upper surface of interface B.

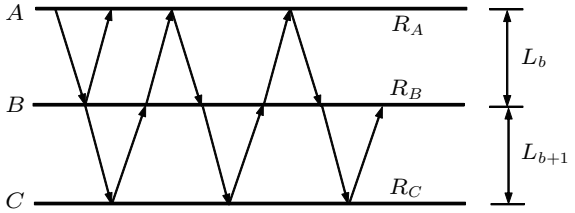


Fig. 2. Double-layer radiant intensity transfer model. A is the interface between air and glass, B is the interface between liquid and glass, C is the interface between liquid and air, subscript b means #b medium layer, $b+1$ means #$(b+1)$ medium layer.

The total proportion of energy that departs from interface A_b and arrives at interface C_{b+1} can be obtained as follows:[22]

$$E_{A_b,b\sim b+1}^{C_{b+1}} = \tau_{b,b+1}F_{A_b}^{B_b}F_{B_{b+1}}^{C_{c+1}}/(1-\beta_2^s), \quad (4)$$

where $\beta_2^s = \tau_{b,b+1}F_{B_{b+1}}^{B_{b+1}}\tau_{b+1,b}F_{B_b}^{B_b}$, $\tau_{b,b+1}$ is the transmittance when the light enters into medium $b+1$ from medium b; $\tau_{b+1,b}$ is the transmittance when the light enters into medium b from medium $b+1$; R_A, R_B, and R_C are respectively the reflectance on the three interfaces A, B, and C; $R_A = R_1 = R_2$, $R_B = R_3$, and $R_C = R_4$. In addition, $\tau_{b,b+1} = \tau_{b+1,b} = 1-R_B$.

When the glass tank contains liquid, the overall transmittance measured by the spectrograph can be expressed as

$$\tau_5 = E_{A_b,b\sim b+1}^{C_{b+1}}(1-R_1)(1-R_4). \quad (5)$$

Let

$$\begin{cases} P_1 = F_{A_b}^{B_b}\tau_{b,b+1}, \\ P_2 = F_{B_b}^{B_b}\tau_{b,b+1}\tau_{b+1,b}, \\ P_3 = E_{A_b,b\sim b+1}^{C_{b+1}}, \\ Q = \exp(-k_{b+1}L_{b+1}), \end{cases} \quad (6)$$

where k_{b+1} is the absorption coefficient of the liquid and L_{b+1} is the thickness of the liquid layer. By establishing a correlation according to formula (4), the following quadratic equation with one unknown is obtained by conversion:

$$(P_3\cdot R_B\cdot R_C + P_3\cdot P_2\cdot R_C)Q^2 + P_1\cdot Q - P_3 = 0. \quad (7)$$

As L_{b+1} is the known liquid layer thickness, taking the plus sign, k_{b+1} can be derived from

$$k_{b+1} = -\ln(Q)/L_{b+1}. \quad (8)$$

After the reflectance is calculated, the refractive index data of the pure water and quartz[23] and the ionic liquids[24] are obtained. In order to account for all the possible influential factors during the absorption coefficient inversion, formula (8) is always adopted for calculations.

2.2. Propagated uncertainties in absorption coefficient inversion

In order to analyze the effects of the relevant influential factors on the absorption coefficient inversion, the square root synthesis method is used to analyze the propagated uncertainties. The basic formula employed is

$$\frac{\Delta N}{N} = \sqrt{\left(\frac{\partial \ln f}{\partial x_1}\right)^2\Delta x_1^2 + \left(\frac{\partial \ln f}{\partial x_2}\right)^2\Delta x_2^2 + \left(\frac{\partial \ln f}{\partial x_3}\right)^2\Delta x_3^2 + \cdots + \left(\frac{\partial \ln f}{\partial x_n}\right)^2\Delta x_n^2}, \quad (9)$$

where $x_1, x_2, x_3, \ldots, x_n$ are directly measured parameters independent of each other and each of them must be a parameter that is determined through multiple equal-accuracy measurements and contains a random error; N is an indirectly measured parameter ($N = f(x_1, x_2, x_3, \ldots, x_n)$), and ΔN is the absolute error of the indirect measurement

$$\Delta N = \sqrt{\left(\frac{\partial f}{\partial x_1}\right)^2\Delta x_1^2 + \left(\frac{\partial f}{\partial x_2}\right)^2\Delta x_2^2 + \left(\frac{\partial f}{\partial x_3}\right)^2\Delta x_3^2 + \cdots + \left(\frac{\partial f}{\partial x_n}\right)^2\Delta x_n^2}. \quad (10)$$

During the absorption coefficient inversion process, the error covers the transmittance measurement error of the experimental system, the refractive index error of the sample tank, the refractive index error of the measured liquid, and the measurement error of the liquid layer thickness.

According to the Huang's research findings,[25] the relative error of the calibrated transmission/reflection spectrum measurement system is not greater than 3%. In the study, the transmittance measurement errors in the two cases including empty sample tank and liquid-containing sample tank are considered to be 3%. The value of the quartz glass sample tank's refractive index is obtained from Ref. [23]. Considering that there might be a certain difference between the quartz material of the glass tank and that in the reference, the relative error of the glass tank's refractive index is assumed to be 1% during the uncertainty propagation analysis. The value of the refractive index of each measured liquid is determined by using the SpectroMaster, a fully automatic high-accuracy refractive index measuring instrument from the Technical Institute of Physics and Chemistry, Chinese Academy of Sciences (CAS) and the minimum deviation angle method, with the relative error smaller than 1.0×10^{-4} (high-accuracy). This ensures that the influence of the liquid's refractive index error cannot be considered during the analysis. A Vernier caliper with an accuracy of 0.05 mm is used to measure the thickness of the liquid layer. The liquid thickness is assumed to be 0.25 cm and the liquid layer thickness error is smaller than 2%.

Two measurement cycles are carried out respectively for the two cases, i.e., empty sample tank and liquid-containing sample tank. The measurement errors are denoted as τ_2 and τ_5, and the following uncertainty propagation formula (11) is used when the absolute error is analyzed during the absorption coefficient measurement:

$$\Delta k_{b+1}=\sqrt{\left(\frac{\partial k_{b+1}}{\partial n_{\text{glass}}}\right)^2\Delta n_{\text{glass}}^2+\left(\frac{\partial k_{b+1}}{\partial \tau_2}\right)^2\Delta\tau_2^2+\left(\frac{\partial k_{b+1}}{\partial \tau_5}\right)^2\Delta\tau_5^2+\left(\frac{\partial k_{b+1}}{\partial L_{b+1}}\right)^2\Delta L_{b+1}^2}. \tag{11}$$

When multiple reflections are considered, the following formula can be obtained:

$$k_{b+1}=\ln\left[2P_3\left(R_BR_C+P_2R_C\right)\Big/\left(-P_1+\sqrt{P_1^2+4P_3^2\left(R_BR_C+P_2R_C\right)}\right)\right]/L_{b+1}. \tag{12}$$

We substitute n for n_{glass} in formula (11). The parameter n here still represents the glass's refractive index.

We define a parameter W_P as

$$W_P=\sqrt{P_1^2+4WP_3}, \tag{13}$$

then the right side of formula (11) can be obtained based on the following expressions:

$$\begin{cases}\dfrac{\partial k_{b+1}}{\partial n}=\dfrac{1}{L_{b+1}}\left(\dfrac{1}{W}\dfrac{\partial W}{\partial n}-\dfrac{1}{-P_1+W_P}\left(\dfrac{2\partial P_1}{\partial n}+\dfrac{1}{W_P}\right)\left(P_1\dfrac{\partial P_1}{\partial n}+2P_3\dfrac{\partial W}{\partial n}+2W\dfrac{\partial P_3}{\partial n}\right)\right),\\ \dfrac{\partial k_{b+1}}{\partial \tau_2}=\dfrac{R_B}{L_{b+1}}\left(\dfrac{\left(W_p-P_1\right)\partial F_{A_b}^{B_b}/\partial\tau_2-2P_3^2R_BR_C\partial F_{B_b}^{B_b}/\partial\tau_2}{W_P^2-P_1W_P}+\dfrac{P_3R_BR_C\partial F_{B_b}^{B_b}/\partial\tau_2}{W}\right),\\ \dfrac{\partial k_{b+1}}{\partial \tau_5}=\dfrac{1}{L_{b+1}}\left(\dfrac{-4W}{W_P\left(W_P-P_1\right)\left(1-R_1\right)\left(1-R_4\right)}+\dfrac{1}{\tau_5}\right),\\ \dfrac{\partial k_{b+1}}{\partial L_{b+1}}=\dfrac{\ln\left[\left(W_P-P_1\right)/2W\right]}{L_{b+1}^2}.\end{cases} \tag{14}$$

The absolute error can be obtained by substituting formula (14) into formula (11). Then, the relative error is obtained through dividing the absolute error by the value calculated with formula (12).

3. Experiment

3.1. Materials

The materials used in this study were C_3MImI and its four derivatives including C_4MImI (methyl butyl imidazole iodide), C_5MImI (methyl pentyl imidazole iodide), C_3MImBr (methyl propyl imidazole bromide), and C_3MImBF_4 (methyl propyl imidazole tetrafluoroborate). All the ionic liquids were purchased from the Lanzhou Institute of Physical Chemistry, CAS.

3.2. Principle and methods

For the incident radiation energy and emission radiation energy, a detector was used with a lock-in amplifier to amplify the measured signal, extract the effective signal, and convert it into a corresponding voltage signal. The corresponding value of the voltage was calculated as $U=K\phi I_\lambda\eta_\lambda\Delta\lambda$, where K is the number of geometric gathers of the system, ϕ is the responsive efficiency of the lock-in amplifier, I_λ is the spectral radiation intensity, η_λ is the spectral responsiveness of the detector, and $\Delta\lambda$ is the bandwidth of the radiation source. When

the voltage response to the incident and emitting light source signal was obtained, the transmittance of the sample can be calculated from $T_\lambda = U_\mathrm{i}/U_0$, where U_i is the voltage response to the spectral emitting signal, and U_0 is the voltage response to the incident signal. The calibration and error analysis of the transmission spectrum measurement system were carried out according to the scheme previously published in Ref. [25] and will not be elaborated here. The literature indicates that the maximum relative error of the calibrated system is no more than 3%.

3.3. Apparatus

An existing transmission spectrum measurement and control system was used. In the experiment, its transmittance measurement function was mainly used to measure the light transmittances of the ionic liquids under external voltages and their changes. The measurements were conducted in a dark environment at normal temperature and pressure.

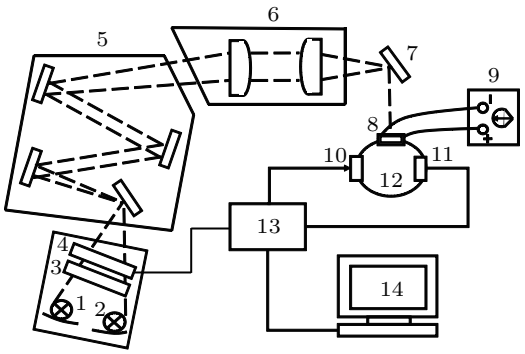


Fig. 3. Illustration of a measurement system for transmission spectrum. Here, 1: deuterium lamp, 2: tungsten lamp, 3: optical filter, 4: chopper, 5: monochromator with double grating, 6: collimating lens, 7: flat mirror, 8: sample holder, 9: voltage adjustable DC power supply, 10: silicon detector, 11: InGaAs detector, 12: integrating sphere, 13: lock-in amplifier, and 14: data acquisition system.

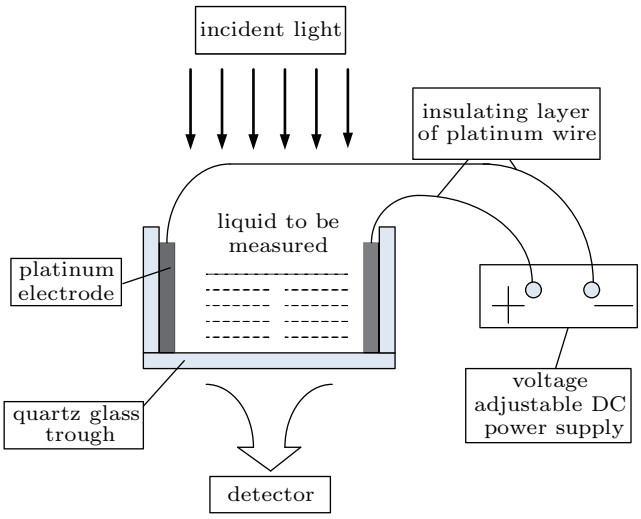


Fig. 4. Electronically controlled ionic liquid transmittance measurement.

The principle and physical diagram of the transmission spectroscopy used are shown in Fig. 3. The system can be used to measure the transmittances of the liquid layer at different voltages. Secondly, this system can provide a stable and smooth continuous light source, and has the characteristics of good measurement repeatability, a small influence of stray light, and high accuracy of signal-to-noise ratio measurement.

The experimental apparatus is sketched in Fig. 4. The incident light passed through the measured liquid and the sample tank perpendicularly and was received by the detector. The signal was amplified by the lock-in amplifier, and then the transmittance was outputted to a computer terminal after the automatic software calculation had been performed.

3.4. Procedure

The experimental procedure included the calibration, the transmittance measurement of empty glass tank and ionic liquid. After that, the absorption coefficient inversion and error analysis were conducted. During the calibration, the outlet passage of the monochromator was aligned on the same horizontal line as the detector's receiving passage. The grating was adjusted to an appropriate position to ensure that the lock-in amplifier's signal was maximum. During the transmittance measurement of the empty glass, comparison measurements were conducted under the deuterium lamp when no sample was provided and the deuterium lamp in the 380–2500 nm band when a sample was provided. Then, the current response was measured under the tungsten lamp when no sample was provided. Eventually, the transmittance was calculated by using the instrument's built-in algorithm.

An appropriate amount of measured liquid was taken using an injector with 0.025 ml graduation and injected into the sample tank. The spacing between positive and negative electrodes was 5 cm. The liquid was allowed to uniformly spread without any bubbles for 10–20 min in the sample tank. In the process, a micrometer was used to make sure that the liquid layer's thickness was 0.25 cm. In the cases when the liquid layer was too thick or too thin, a tiny amount of the liquid was take away from or inject into the sample tank correspondingly. When the liquid layer became stable, the positive and negative poles of the voltage adjustable DC power supply were connected to the platinum wires of the sample tank respectively. The voltage on the power supply was then set to be zero. The sample tank containing the liquid was taken into the transmittance measurement chamber of the spectrograph and the transmittance of the entire apparatus containing the liquid was measured. After each set of measurement data was obtained, the power supply voltage was adjusted by slowly rotating the knob to allow the voltage to gradually increase from zero. In order to ensure that the voltage is not high enough to electrolyze the ionic liquid, the experimental measurement voltages are required to include 0 V, 0.5 V, 1 V, 1.5 V, 2 V, 2.5 V, 3 V, and 3.5 V. Given the electrode spacing of 5 cm,

the corresponding electric field intensities are 0 V/m, 10 V/m, 20 V/m, 30 V/m, 40 V/m, 50 V/m, 60 V/m, and 70 V/m, respectively. The apparatus automatically recorded the curve of liquid's transmittance versus wavelength under each of these voltages. In the voltage increase process, the voltage could not decrease at any time. Before each new measurement was made, the system current voltage was kept for a period of 3 min. The measurement procedure was done in an ascending order of voltage. The experiments were carried out under room temperature conditions (20 °C) and one atmosphere (1 atm).

The absorption coefficient inversion process completed in the study was not related to the wavelength. It was related to only five factors including the overall transmittance, empty sample tank's transmittance, sample tank's refractive index, liquid's refractive index, and liquid layer thickness. In order to analyze the overall error of the system in the space controlled by the five factors, the upper/lower limit analysis method was employed.

The overall transmittance was assumed to change continuously only in the 0.05–0.85 range. The sample tank's spectral transmittance ranged from 0.918 to 0.928 with the lower limit assumed to be 0.918 and the upper limit assumed to be 0.928. Similarly, the quartz sample tank's spectral refractive index ranged from 1.4 to 1.5, while the measured liquid's spectral refractive index was assumed to range from 1.05 to 2.0. The liquid layer's thickness was taken to be 0.25 cm. Based on the above values, the total transmittance was continuously changed, and 8 limiting conditions were constructed. The detail of the calculation conditions is listed in Table 1.

Table 1. Detail of eight typical cases of calculation conditions.

	Case 1	Case 2	Case 3	Case 4	Case 5	Case 6	Case 7	Case 8
n_{glass}	1.5	1.4	1.5	1.4	1.5	1.4	1.5	1.4
n_{liquid}	2	2	1.05	1.05	2	2	1.05	1.05
τ_{glass}	0.928	0.928	0.928	0.928	0.918	0.918	0.918	0.918

According to the parameters listed in the table, the relationships of the inversion relative error of the absorption coefficient and the corresponding absorption coefficient with the total transmittance are obtained respectively as shown in Fig. 5. As can be seen, the relative error of the absorption coefficient measurement increases with transmittance increasing. When the transmittance is no less than the lowest sensitivity of the experimental equipment, the larger the absorption coefficient, the smaller the relative measurement error. For the band with larger absorption coefficient, the transmittance can be maintained in the appropriate range by changing the thickness of the liquid layer. In addition, it can be seen that the relative error of the absorption coefficient caused by the above factors is less than 15% when the absorption coefficient is greater than 0.5 cm^{-1}. Considering the fact that the test factors do not change during a set of tests for each liquid to be tested, the above errors are a conformity error.

The ionic liquid used in this work had a purity of better than 99.5%. Since this paper focuses on the unique phenomenon of the change of the absorption coefficient of ionic liquid under electric field, rather than the calibration of the pure ionic liquid absorption coefficient, the effects of impurities on the spectral curve will not be discussed.

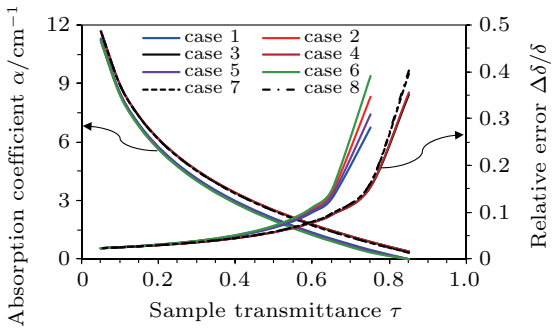


Fig. 5. Plots of absorption coefficient and the inversion relative error versus sample transmittance.

4. Results and discussion

The absorption coefficients of the five kinds of ionic liquids are calculated according to the measured transmittance values, and the curves of absorption coefficient versus wavelength at different voltages are plotted. Under the electric field, the elementary experiment shows that as long as the voltage does not exceed the threshold of the decomposition of the ionic liquid, the test results are reproducible at the same voltage. However, the voltage thresholds of decomposition of the ionic liquids before the experiment are unknown. It is assumed that the amount of liquid was constant during the test and the ionic liquid did not break down as the voltage gradually increased, thus the voltage in the test was increased step by step (the step size is 0.5 V).

The absorption coefficients of the different ionic liquids at 0 V and 1 V are compared in Fig. 6. As shown in the figure, there are clear differences in the absorption coefficient versus wavelength among the different ionic liquids. The effects of the applied voltage on the absorption coefficient are also varying for the different ionic liquids. The changes in absorption coefficients of ionic liquids under atmosphere and electric field at different wavelengths are different. For investigating these changes in detail, the absorption coefficient maps versus wavelength are provided in Fig. 6.

The absorption coefficients of C_3MImI versus wavelength under different electric fields are shown in Fig. 7. It can be seen that at 1440 nm and 1960 nm, the absorption coefficient increases markedly as the intensity of the applied electric field increases. The absorption coefficient at 1520 nm is increased by 114% and that at 1960 nm by 328.1% as the voltage increases from 0 V to 3.5 V. Inversely, neither of the absorption coefficients in two bands of wavelength (400–430 nm, 1675–1735 nm) presents a clear trend with the applied voltage increasing. Note that the absorption coefficient at 1 V is the

largest, whereas the absorption coefficient at 2 V near to the ultraviolet band is the smallest and at 3.5 V near the infrared band is also the smallest.

The plots of absorption coefficient of C_4MImI versus wavelength under an applied electric field are shown in Fig. 8. It can be seen that when the wavelength is shorter than 1400 nm, the absorption coefficient still does not change considerably with the applied voltage increasing, which is related to the electric field intensity. At 1440 nm and 1960 nm, the absorption coefficients increase markedly as the intensity of the applied electric field increases. The absorption coefficient at 1520 nm is increased by 99% and that at 1960 nm by 141% as the voltage increases from 0 V to 3.5 V. In addition, it is found that the absorption coefficient changes most dramatically when the voltage increases from 0.5 V to 1 V. However, the absorption coefficient is independent of the applied electric field in the two bands of wavelength (400–430 nm, 1700–1740 nm). Note that the absorption coefficient under a 3 V voltage is the largest in the band of 400–430 nm, and it under a 1.5 V voltage is the largest in the band of 1700–1740 nm.

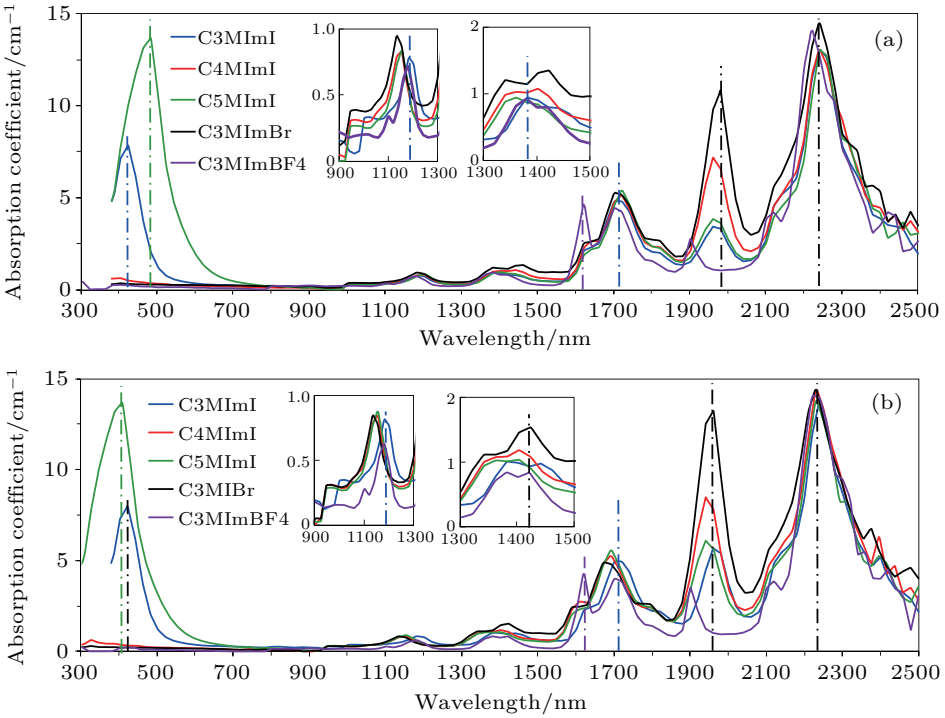


Fig. 6. Comparison of absorption coefficient between different ionic liquids at (a) 0 V and (b) 1 V.

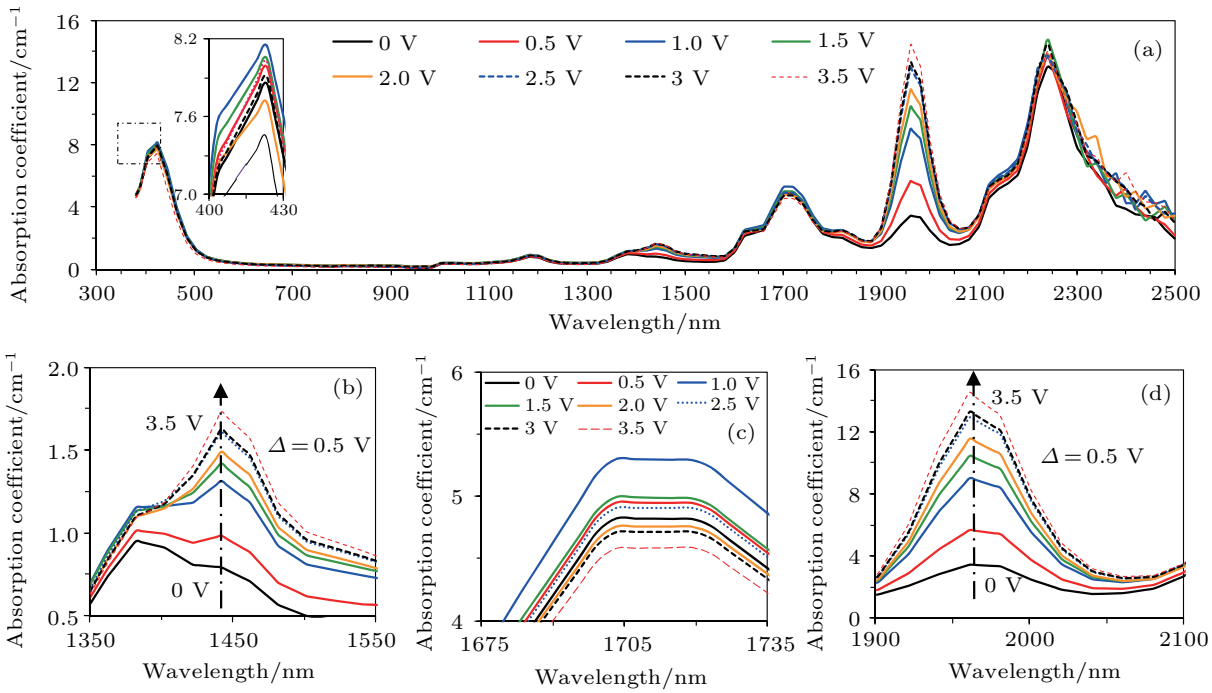


Fig. 7. Plots of absorption coefficient of C_3MImI versus wavelength at different voltages: (a) original map and (b)–(d) local magnification maps.

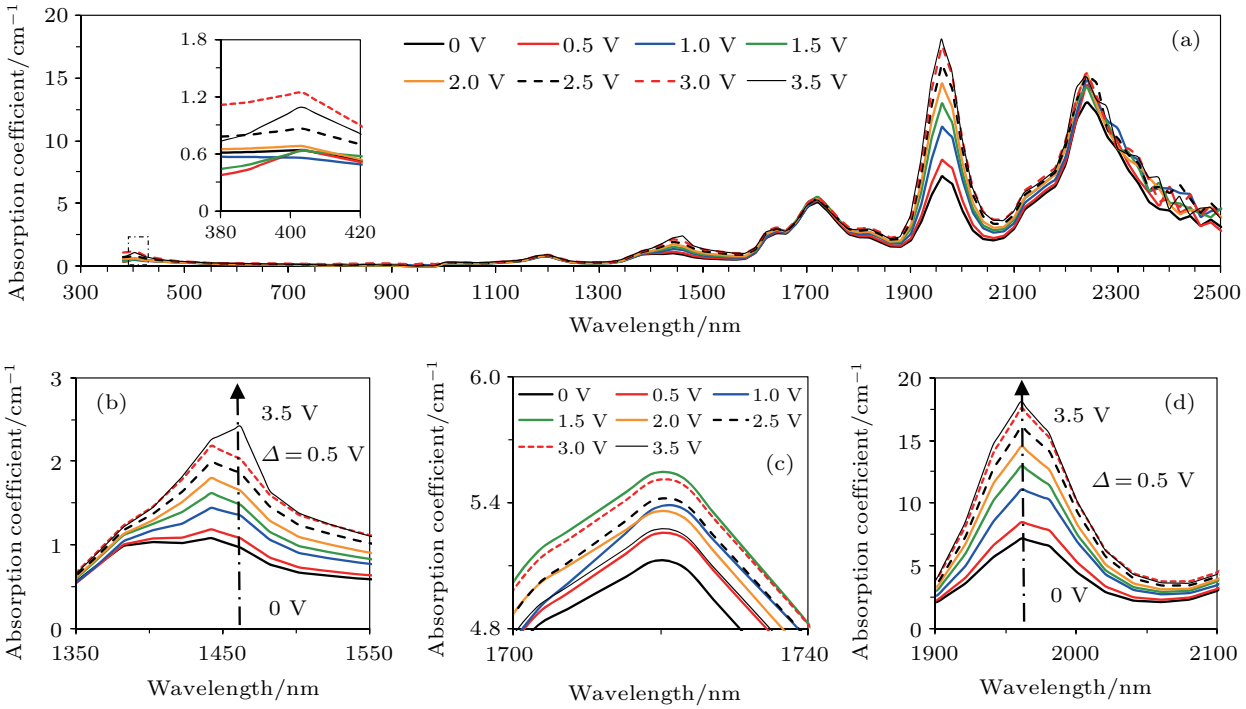


Fig. 8. Plots of absorption coefficient of C_4MImI versus wavelength at different voltages: (a) original map and (b)–(d) local magnification maps.

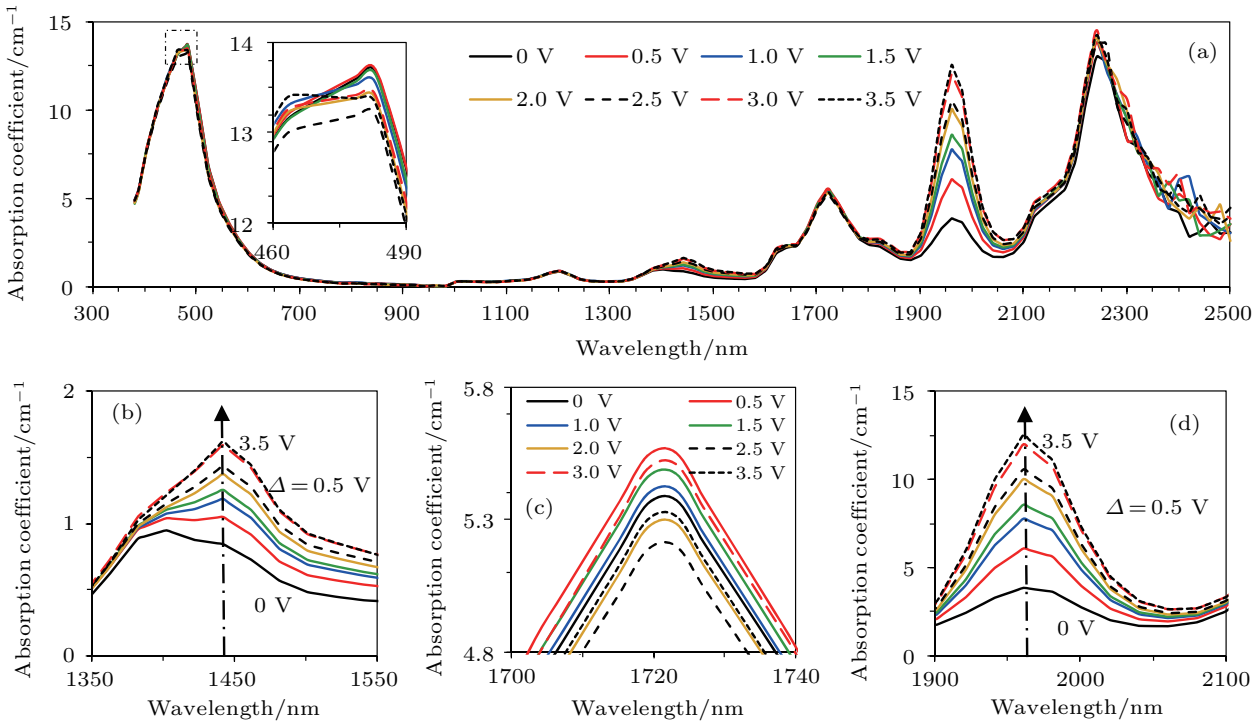


Fig. 9. Plots of absorption coefficient of C_5MImI versus wavelength at different voltages: (a) original map and (b)–(d) local magnification maps.

The plots of absorption coefficient of C_5MImI versus wavelength under different applied electric fields are illustrated in Fig. 9. It can be seen that at 1440 nm and 1960 nm, the absorption coefficients increase markedly as the intensity of the applied electric field increases. Furthermore, there are several regions of wavelength for C_5MImI, which divide the curves of absorption coefficient versus wavelength at different applied voltages. Note that the absorption coefficient increases obviously with the applied voltage increasing in bands of 1350–1550 nm and 1900–2100 nm. However, this situation does not exist in the band of 460–490 nm nor in the band of 1700–1740 nm any more.

The plots of absorption coefficient of C_3MImBr versus wavelength under different applied electric fields are shown in Fig. 10. It can be seen that at 1440 nm and 1960 nm, the absorption coefficients increase markedly as the intensity of

the applied electric field increases. At 1520 nm, the absorption coefficients at 0 V, 0.5 V, 1 V, 1.5 V, 2 V, 2.5 V, 3 V, and 3.5 V are respectively 1.018 cm^{-1}, 1.092 cm^{-1}, 1.315 cm^{-1}, 1.504 cm^{-1}, 1.643 cm^{-1}, 1.775 cm^{-1}, 1.953 cm^{-1}, and 1.984 cm^{-1}. This indicates that the absorption coefficient is increased by 91.8% when the voltage increases from 0 V to 3 V. In the above band, the absorption coefficient at 1460 nm is the maximum and is increased by 124% when the voltage increases from 0 V to 3 V. At 1960 nm, the absorption coefficients at 0 V, 0.5 V, 1 V, 1.5 V, 2 V, 2.5 V, 3 V, and 3.5 V are respectively 10.885 cm^{-1}, 13.948 cm^{-1}, 17.844 cm^{-1}, 20.294 cm^{-1}, 21.789 cm^{-1}, 23.037 cm^{-1}, 24.001 cm^{-1}, and 24.510 cm^{-1}, and the absorption coefficient is increased by 120% when the voltage increases from 0 V to 3 V.

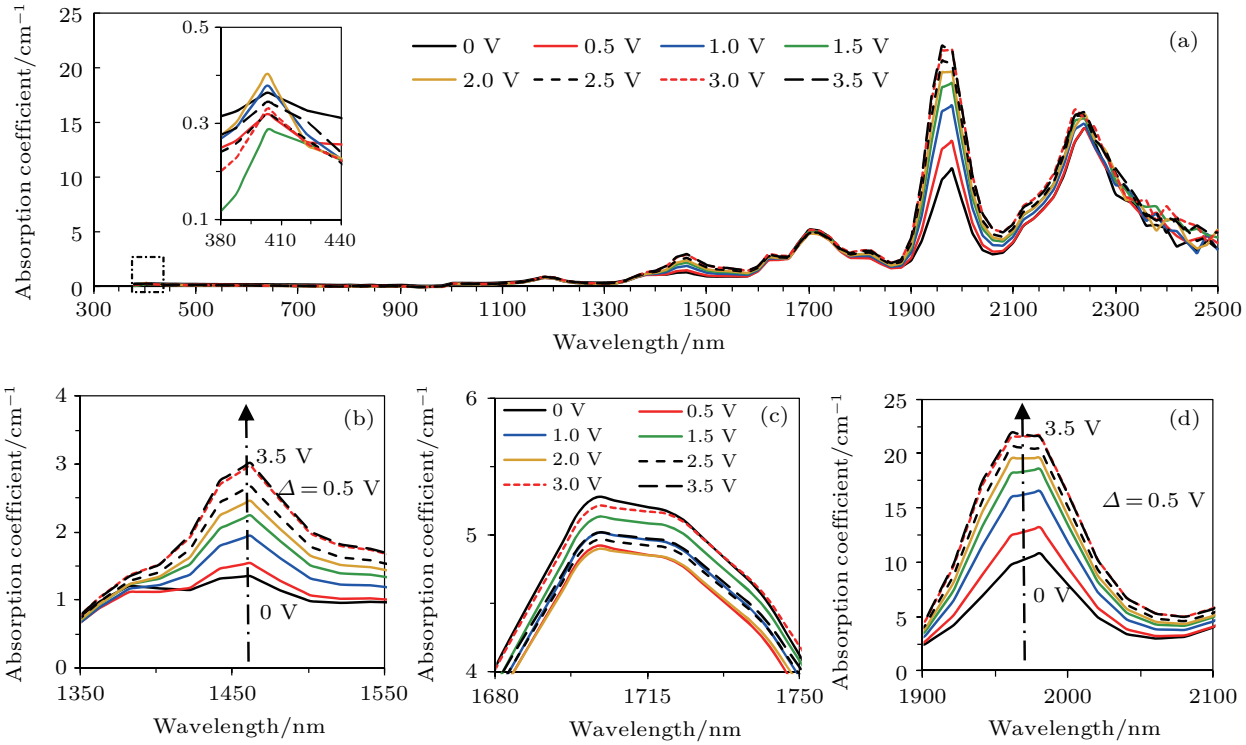


Fig. 10. Plots of absorption coefficient of C_3MImBr versus wavelength at different voltages: (a) original map and (b)–(d) local magnification maps.

The plots of absorption coefficient of C_3MImBF_4 versus wavelength under different applied electric fields are shown in Fig. 11. It can be seen from the figure that the existence of the radical BF_4 brings about a spectral structure different from those of the several working media above. In general, the absorption coefficient at 1440 nm does not change considerably and that at 1960 nm gradually increases when the voltage increases. Taking 1920 nm for example, the absorption coefficients at 0 V, 0.5 V, 1 V, 1.5 V, 2 V, and 2.5 V are respectively 2.206 cm^{-1}, 2.458 cm^{-1}, 3.253 cm^{-1}, 3.730 cm^{-1}, 4.368 cm^{-1}, and 4.736 cm^{-1}. It can be seen that during the voltage increasing from 0 V to 2.5 V, the absorption coefficient is increased by 114%. In addition, it can also be seen that the inversion for obtaining the absorption coefficient is impossible due to the sharp reduction in transmittance in the band 1880–1960 nm and beyond 2100 nm when the voltage increases to 3 V or 3.5 V. The samples change their colors when the voltage increases to 3 V or 3.5 V. This may be due to the high voltage which is beyond the electrochemical window of the ionic liquid and the high voltage allows the ionic liquid to be subjected to ionization breakdown. Therefore, the voltage in the experiment must be controlled within 2.5 V.

According to a comprehensive analysis of the experimental data, the absorption coefficient rankings by anion substituent when no voltage is applied and the incident light's wavelength is 1520 nm and 1960 nm are as follows: C_3MImBr > C_3MImI > C_3MImBF_4. However, the absorption coefficient has different rankings by carbon chain length at different wavelengths. It has the following ranking: C_4MImI > C_3MImI > C_5MImI at 1520 nm, whereas C_4MImI > C_5MImI> C_3MImI at 1960 nm.

In order to compare the absorption coefficient changes of the different ionic liquids under an applied electric field, the ratio of the absorption coefficient α with an applied electric field to the absorption coefficient α_0 without an applied electric field defined as the effect coefficient of the applied electric field is determined. The ratio represents the absorption coefficient under a given electric field and that under 0 V/m reflects the degree of influence of the electric field on the absorption coefficient. Thus, the changes of the absorption coef-

ficients at 1520 nm and 1960 nm under different uniform electric fields are plotted in Fig. 12. The ionic liquid absorption coefficient versus the applied voltage is analyzed. The absorption coefficients change multiple times at the same voltage and are ranked by the carbon chain length as follows: C_3MImI > C_5MImI > C_4MImI. Besides, the absorption coefficients change multiple times at the same voltage ranked by anion as follows: C_3MImI > C_3MImBr > C_3MImBF$_4$.

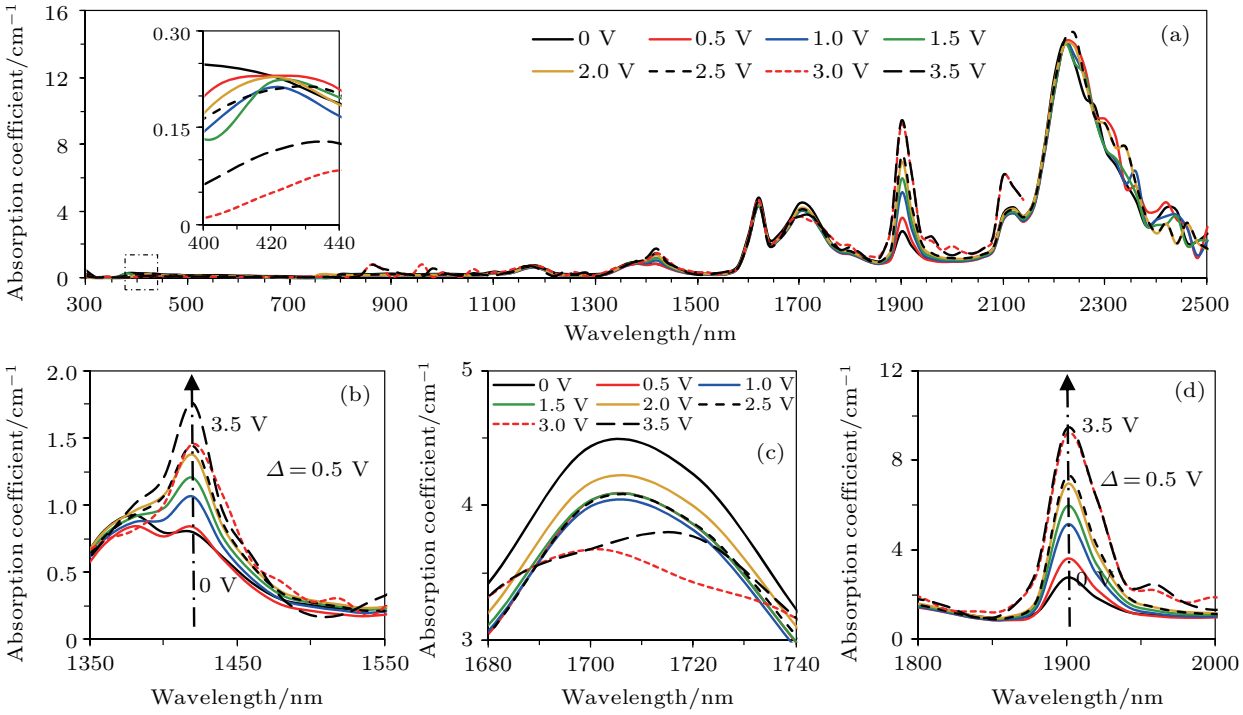


Fig. 11. Plots of absorption coefficient of C_3MImBF$_4$ versus wavelength at different voltages: (a) original map and (b)–(d) local magnification maps.

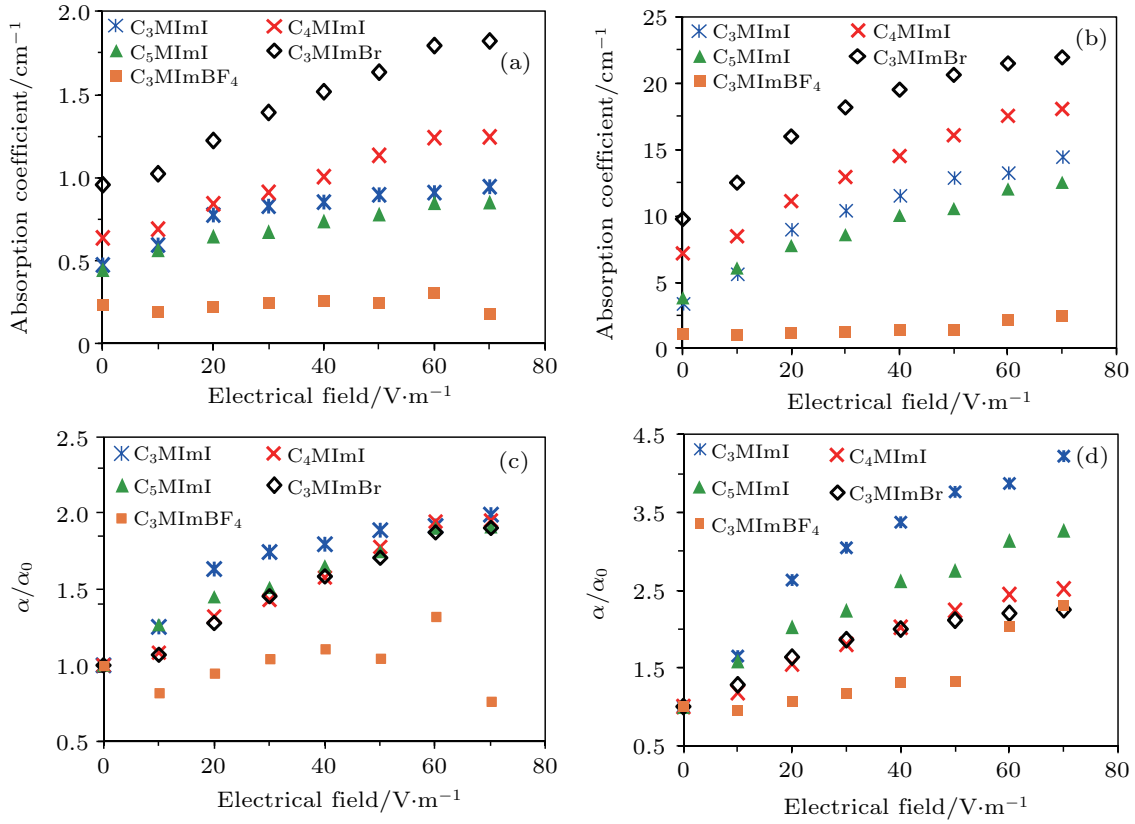


Fig. 12. Comparison of absorption coefficient and the electric effects for two wavelengths at different voltages: (a) absorption coefficient at 1520 nm, (b) absorption coefficient at 1960 nm, (c) α/α_0 at 1520 nm, (d) α/α_0 at 1960 nm.

The above curves show that the absorption coefficient change with voltage is largely dramatic (steep curve) when the electric field is lower than 20 V/m and tends to be gradually gentler (gentle curve) when the voltage is higher than 20 V/m. This is mainly because the ion motions (ion chain formation, ion clustering, etc.) and the anion and cation concentrations are changed or affected initially under the low electric field. Importantly, the distribution pattern and motion state of the ions tend to be steady under the high electric field (before the ionic liquid is decomposed). Besides, many alien charges at electrodes lead to higher ion migration resistances toward both electrodes, thus inhibiting further arrangement and migration of the ions as well as reducing the change of the absorption coefficient with the intensity of the applied electric field.

Differences of absorption coefficients versus voltage for several ionic liquids may explain the physicochemical properties. The bond energy between carbon chain and imidazole ring in C_3MimI is lower than that in C_5MImI and C_4MImI. Under an electric field, C_3MimI having the smaller ion migration resistance is affected significantly by the applied electric field. When no electric field is applied, the C_4MImI's absorption coefficient is higher than that of C_3MImI and C_5MImI. After that, the effect of the applied electric field on the absorption coefficient of C_4MImI is not significant. Under an electric field, the separation of cation-imidazole ring of C_3MImI is easier because the cations are difficult to oxidize, and therefore the effects of the applied electric field are more significant. Differently, the cations of C_3MImBF_4 are easy to oxidize, the separation of the cation-imidazole ring is relatively hard under an electric field, and therefore the influence of the electric field on C_3MImBF_4 is smaller.

5. Conclusions

We have investigated the light transmission properties of ionic liquids in a uniform electric field. A rectangular glass tank with electrodes on both sides is designed to measure the transmittance. An experimental program for measuring light absorption properties of ionic liquids in ultraviolet, visible, and near-infrared spectrum ranges is also developed. Five kinds of imidazole ionic liquids' spectrum absorption coefficient versus electric field intensity laws are identified and illustrated. Multiple refractions and reflections are considered in the process of absorption coefficient inversion. An analysis of propagated uncertainties involved in the measurement results is carried out by using the uncertainty propagation formula for the absorption coefficient and determining the error range of the inversion results. The main conclusions obtained are as follows.

(i) Near 1520 nm and 1920 nm, the absorption coefficient gradually increases as the voltage increases. Specifically, the peak value of absorption coefficient occurs at 1920 nm. In the short-wavelength range, the absorption coefficient changes very slightly with the voltage range. Within the above bands, the descending-order rankings in absorption coefficient's susceptibility to the applied electric field by carbon chain length and cation are respectively as follows: C_3MImI > C_5MImI > C_4MImI and C_3MImI > C_3MImBr > C_3MImBF_4.

(ii) The accuracy of the absorption coefficient measurement is affected by the system's inherent transmittance measurement error, the sample tank's refractive index error, the liquid layer's refractive index error, and the liquid layer thickness error. When the relative error of the transmittance measurement is smaller than 3%, the relative errors of the glass tank's refractive index and the liquid's refractive index are smaller than 1% and 0.1%, respectively. The liquid thickness-induced error is also smaller than 2%. When the relative error of the transmittance measurement is smaller than 3%, the relative errors of the glass 4 tank's refractive index and the liquid's refractive index are smaller than 1% and 0.1%, respectively. The liquid thickness induced error is also smaller than 2%. When the absorption coefficient is greater than 0.5 cm^{-1}, the absorption coefficient relative error caused by the above factors is controlled within 15%.

(iii) The absorption coefficient changes dramatically with the voltage in the beginning and then tends to change slightly as the voltage continues to increase. This proves that there is a specific connection between the ion migration and absorption coefficient change.

This study can provide experimental means and data support for further mechanism analysis and theoretical simulations of ionic liquids' electro-optical effect. It provides strong support for the electro-optical regulation technologies used in a number of fields such as optical communication, optical sensing, optical displaying, high-power solid laser, smart glass, solar PV generation, etc. It also lays the foundations for further exploring the electro-optical regulation mechanisms and capabilities of ionic liquids, ionic liquid-like soft materials, and metamaterials.

References

[1] Hu W, Zhang L, Cao H, Song L, Zhao H, Yang Z, Cheng Z, Yang H and Guo L 2010 *Phys. Chem. Chem. Phys.* **12** 2632

[2] Wang F, E Itkis M E, Bekyarova E, *et al.* 2013 *Nat. Photon.* **7** 459

[3] He B, Zhang C H and Ding A 2017 *Chin. Phys. B* **26** 126102

[4] Liu H X, Man R L, Zheng B S, Wang Z X and Yi P G 2014 *Chin. J. Chem. Phys.* **27** 144

[5] Lu L Y, Zhang Y J, Chen J J, *et al.* 2017 *Chin. J. Chem. Phys.* **30** 423

[6] Ding S, Wei L G, Li K L and Ma Y C 2016 *Chin. J. Chem. Phys.* **29** 497

[7] Du L K, Geng C H, Zhang D J, Lan Z G and Liu C B 2016 *J. Phys. Chem. B* **120** 6721
[8] Song Y Y, Tian P and Yu L 2013 *Adv. Mater. Res.* **772** 219
[9] Yang Q 2014 *Appl. Mech. Mater.* **685** 106
[10] Yu L and Tian P 2014 *Appl. Mech. Mater.* **685** 98
[11] Paul A, Mandal P K and Samanta A 2005 *J. Phys. Chem. B* **109** 9148
[12] Paul A, Mandal P K and Samanta A 2005 *Chem. Phys. Lett.* **402** 375
[13] Paul A, Mandal P K and Samanta A 2006 *J. Chem. Sci.* **118** 335
[14] Jo T S, Koh J J, Han H and Bhowmik P K 2013 *Mater. Chem. Phys.* **139** 901
[15] Zhang L, Liu J, He G D, Ye Z C, Fang X M, Zhang Z G 2014 *Sol. Energy Mater. Sol. Cells* **130** 521
[16] Ansari S A, Liu L S and Rao L 2015 *Dalton Trans.* **44** 2907
[17] Hu W, Zhao H, Song L, Yang Z, Cao H, Cheng Z, Liu Q and Yang H 2010 *Adv. Mater.* **22** 468
[18] Nakano M, Shibuya K, Ogawa N, Hatano T, Kawasaki M, Iwasa Y and Tokura Y 2013 *Appl. Phys. Lett.* **103** 153503
[19] Reddy B N and Deepa M 2013 *Polymer* **21** 5801
[20] He X D, Shao Q F, Cao P F, Kong W J, Sun J Q, Zhang X P and Deng Y Q 2015 *Lab Chip* **15** 1311
[21] Fu T R, Liu J F 2015 *Infrared Phys. Techn.* **69** 88
[22] Lou J F 2002 *Transient coupled heat transfer in multilayer absorbing-scattering composite with specular and diffuse reflection properties* (Ph. D. Dissertation) (Harbin: Harbin Industrial University) (in Chinese)
[23] David R L 1989 *Handbook Chem. Phys.* (69th Edn.) (Boca Raton: CRC Press) p. E382
[24] Zhou J 2015 *Research on the optical transmission characteristics and electrical modulation mechanism of electro-optic material under multi field effect* (Ph. D. Dissertation) (Harbin: Harbin Industrial University) (in Chinese)
[25] Huang X 2016 *Photo-thermal characteristics analysis for concentrating radiation thermal decomposition process based on ferrite* (Ph. D. Dissertation) (Harbin: Harbin Industrial University) (in Chinese)